Communications

# Hollow Microtubes and Shells from Reactant-Loaded Polymer Beads**

Rabih Makki, Mohammed Al-Humiari, Sumana Dutta, and Oliver Steinbock

The production of complex micrometer-scale structures by spatial control of chemical reactions and physical transformations is unambiguously demonstrated by living systems. For example, certain marine algae surround themselves with intricate arrays of calcite-based plates or tubes, while radiolarians stabilize their extravagant shapes with internal microspikes and perforated shells made of silica.[1] These structures are clearly the result of complicated and genetically regulated cellular functions, but also involve generic physicochemical mechanisms that create spatial complexity from emergent phenomena. These nonequilibrium phenomena should also exist in nonbiological systems, but the number of examples established to date is quite small.[2]

In chemistry, the production of nano- and microstructures with complex shapes typically relies on sol–gel, precipitation and other solidification processes such as vapor deposition. Classic examples of macroscopic complexity are Liesegang rings and the formation of so-called "silica gardens". The latter example is known to many as a chemistry toy and demonstration experiment, and leads to millimeter-sized, hollow tubes in aqueous solutions of silicates, borates, or carbonates from small, submerged salt seeds.[3] Most common inorganic compounds can be used as seed particles with the exception of alkali-metal salts. Hollow precipitation tubes are also observed on corroding metals, in setting cement, in caves as "soda straw" speleotherms, and on the ocean floor as "black smokers".[4] The length scales of these tubular precipitation structures span three orders of magnitude. Ritchie et al. recently studied silica tube formation from small polyoxometalate-based solid grains and observed tube radii as small as several micrometers.[5] Even smaller silica tubes (0.1 μm) have been synthesized using organic-crystal templating and liquid-crystal phase transformations.[6] Clearly, such length scales make these hollow tubes interesting targets for various applications.

Herein, we report a novel approach to silica microstructures. Our approach is based on compartmentalizing the two reactant solutions in a controlled and quantifiable fashion. For these experiments, we produce agarose beads as a microvessel by using a conventional emulsification technique.[7] The gel beads are then loaded diffusively with

copper sulfate and finally exposed to a large volume of sodium silicate solution. The resulting dynamics are illustrated by the brightfield micrographs in Figure 1 (see the
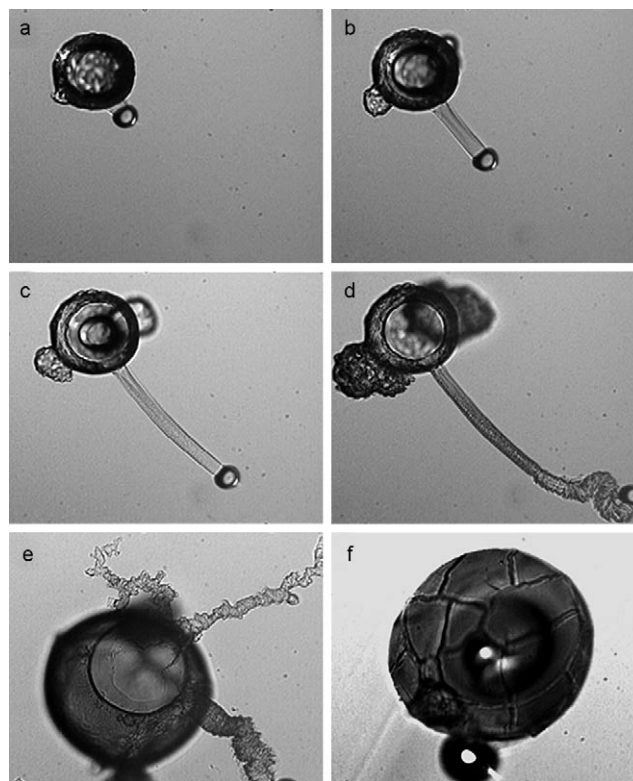
Figure 1. Optical micrographs obtained from three experiments. a–d) Image sequence illustrating microtube growth. Time intervals between frames (a)–(d) are 2.1 s, 2.7 s, and 17.1 s, respectively. [CuSO$_4$] = 1.15 M. e) Formation of multiple tubes from one bead. [CuSO$_4$] = 0.05 M. f) Cracks in a solidifying colloidal shell approximately 12 s after addition of sodium silicate solution. [CuSO$_4$] = 1.0 M. All images show an area of (0.46×0.38) mm^2.

Supporting Information for movies). The first four frames (a–d) are an image sequence of a typical example of microtube growth. The large object is the agrose bead (radius 60 μm) surrounded by an expanding colloidal layer. The smaller round object at the lower right of the bead is an air bubble (radius 18 μm), which is probably formed from gas trapped on the surface of the bead during wetting. The bubble is pinned to the growing microtube and moves away from the gel bead. Careful inspection of faint tube features and their overall shapes allow us to conclude that tube growth always occurs close to the air bubble and neither at the bead nor along the structure. Nonetheless, we always observe a gradual change in

[*] R. Makki, M. Al-Humiari, Dr. S. Dutta, Prof. O. Steinbock
Department of Chemistry and Biochemistry
Florida State University
Tallahassee, FL 32306-4390 (USA)
Fax: (+1) 850-644-8281
E-mail: steinbck@chem.fsu.edu

tube color from translucent, near colorless to a more turbid blue. These changes cease about 25 s after the initial formation, and are likely due to continued polymerization and precipitation reactions on both sides of the tubular wall.

Bubble-assisted growth starts within the first 1–2 s after exposure of the beads to the sodium silicate solution. We also found that the tube radius is closely related to the bubble size, which is typically 80–90% of its radius. A similar bubble-dependent size selection has been observed for macroscopic silica tubes produced by injection methods.[8,9] In the latter experiments, the tubes extend strictly in the vertical direction because of the high buoyancy of the pinned bubble.[9] For microbead-controlled growth, however, tubes have no clear directional preference and the pinned bubbles appear to be aspherical (Figure 1 a–c but not d). Moreover, we found that tube formation is typically accompanied by the growth of nodular objects that differ distinctly from the elongated tube structures (see Figure 1 a–d). The total number of nodules per bead ranges between zero and four.

Hollow microtubes can also form in the absence of attached bubbles (Figure 1 e). These structures usually evolve 30–40 s after initiation of the reaction. They are clearly less linear than their bubble-templated counterparts and grow to full lengths in single, fast bursts. Furthermore, several of these secondary tubes can form from one bead. Under the experimental conditions studied, we observed up to seven tubes per bead, while certain reaction conditions reliably fail to induce tube growth.

Regardless of the number of tubes, we always observed an initially rapid then decelerating radius increase of the reacting bead system. For instance, the radius of the sample in Figure 1 f increased from an initial value of 124 μm to a final value of 151 μm within approximately 25 s and at an initial rate of 3.7 μm s^{-1}. Even larger changes were observed for silicate-loaded beads in copper sulfate solution. In addition, experiments with dried, salt-free agarose beads show unambiguously that this increase is not due to solvent-induced swelling. Instead, we interpret the size increase as the formation of a colloidal layer that surrounds the agrose bead. Perhaps more interestingly, we also observed the formation of intricate crack patterns. These fractures occur approximately 4 s after initiating the reaction. Initially, the fractures appear as short dark lines that grow at both ends to finally form a network of polygons in which the individual fracture lines meet at angles of approximately 90 degrees (see Figure 1 f). Preliminary measurements yield crack velocities of 100–200 μm s^{-1}, which are unusually slow, even for soft materials that have low speeds of sound.[10] In addition, the onset of the fractures must correlate with a sufficiently strong shift from a liquid to a gel-like, solid behavior and might hold useful information on the viscoelastic properties of the expanding shell. We also emphasize that the observed fractures are "self-healing"[11] as fresh colloidal matter will immediately form in the wake of a breach.

Figure 2 a provides more detailed information on the reaction conditions that induce microtube formation. For this analysis, we varied bead radii and copper sulfate concentrations while keeping all other parameters, including the sodium silicate concentration (1.0 mol L^{-1}), constant. The
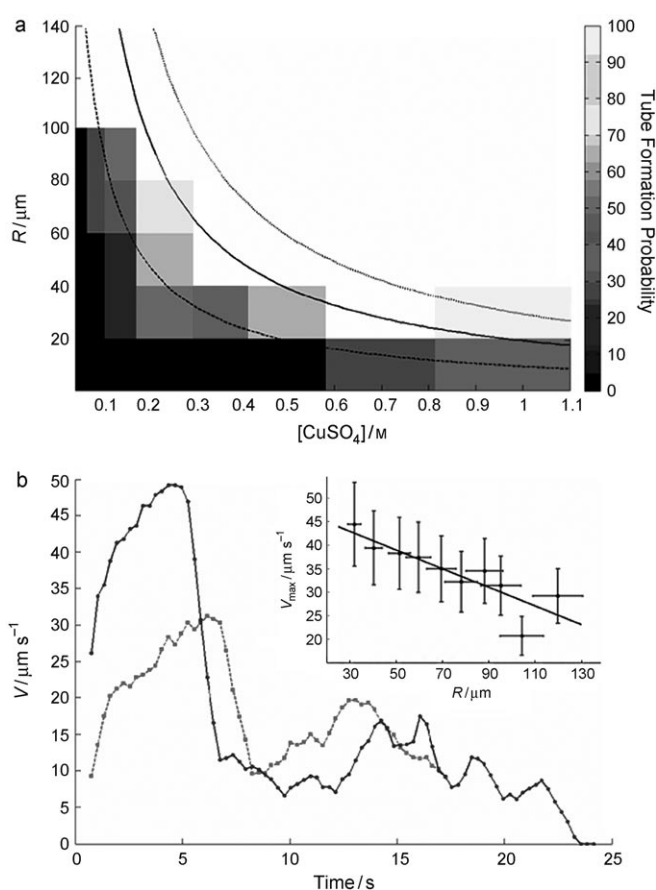
Figure 2. a) Phase diagram showing the tube formation probability as a function of bead radius R and initial copper sulfate concentration. The continuous curves are hyperbolas ($R = k/[CuSO_4]$) that approximate the critical bead radius above which tubes form. The proportionality constant k equals 10, 20, and 30 μm mol L^{-1} for the dashed, solid, and dotted lines, respectively. b) Velocity of the forming tube as a function of time for bead radii of 58 μm (solid line) and 93 μm (dashed line). [CuSO$_4$] = 1.15 M. The inset shows the maximum growth velocity as a function of bead radius at the same concentration. The straight line is the best linear fit.

shades in the phase diagram represent the tube-formation probability as determined by inspection of approximately 500 different beads and appropriate binning of their initial radius and loading concentration. Parameter regions with dark shades indicate that tubes are absent or unlikely to form, while white areas represent conditions in which all beads generated microtubes. These data reveal that high concentrations of copper sulfate and large bead radii favor tube formation. Furthermore, the data suggest that tube growth occurs only above a critical bead radius R_{crit} that is inversely proportional to the initial loading concentration c. This simple dependence (i.e., $R_{crit} = k/c$) is plotted in Figure 2a for proportionality constants k of 10, 20, and 30 μm mol L^{-1}.

The good agreement between this simple relation and our experimental data suggest that the surface-to-volume ratio of the microbead ($3/R$ for a perfect sphere) strongly affects tube formation. This dependence can be explained semiquantitatively by comparing the initial amount of copper ions stored in the bead n_0 to the amount of copper ions n_s consumed during

the formation of a colloidal shell of width w and copper concentration c_s. The actual criterion for tube growth is then $n_0 > n_s$ because copper ions are also needed for assembling the tubular structure. Assuming that the shell is thin ($w \ll R$), we find that $R_{crit} = 3 w c_s/c$. In the context of this simple scaling argument, we can now interpret the value of the constant k as approximately $3 w c_s$. For a width of about 1 μm, this expression yields concentrations c_s in the range of 3–10 M, which is in reasonable agreement with the expected values.[12] We emphasize that we have disregarded reaction-induced concentration gradients within the bead. However, this simplification might be acceptable as the diffusion time $t_d = R^2/(2D)$ is shorter than, or at least similar to, the time required for tube nucleation (e.g., $t_d \approx 0.6$ s for a diffusion constant D of 2×10^{-5} cm^{2}s^{-1} and a typical radius of 50 μm).

While the nucleation of the spherical shells and initial tubes occurred within 1–2 s, tube growth could last for up to 1 min. During this time, the growth speed of the tubular structures was far from constant. Figure 2b shows two typical examples for the velocity evolution of bubble-templated tubes that emerge from beads with radii of 58 μm (solid line) and 93 μm (dashed line). The velocities were always measured from position changes of the gas bubble, and only experiments with stationary beads were analyzed. The maximum growth speed v_{max} was reached within 4–8 s after initiation of the reaction. Depending on the experimental conditions, we measured v_{max} values between approximately 20 and 50 μm s^{-1}. For constant initial concentrations, the value of v_{max} averaged over many experiments decreased with increasing bead radius (see inset of Figure 2b).

The detailed time-dependence of the growth velocity suggests that bubble-guided tube growth often occurs in two distinct stages. During the initial phase, velocities are fast and quickly approach v_{max}. Subsequently, growth continues but at much lower speeds (typically between 5 and 20 μm s^{-1}). This second stage is three to four times as long as the initial one. The intermittent velocity drop is abrupt and can be clearly discerned in the two examples shown in Figure 2b. The velocity drop is sometimes accompanied by the temporary cessation of tube formation.

The rapid switching between fast and slow growth manifests itself in strikingly different tube morphologies. For instance, the first three micrographs in Figure 1 (covering the first 6 s of reaction) correspond to fast growth and show the formation of a straight tube with smooth wall texture. During the following 20 s, however, tube growth is slow and erratic. As shown in the corresponding micrograph (Figure 1d), the tube formed during this time interval has a very different texture and appears to be grainy and segmented.

To obtain further insights into the morphology and surface texture of microtubes and microshells, we imaged numerous samples by scanning electron microscopy (SEM). For this purpose, post-reaction samples were carefully removed from the sodium silicate solution, washed, dried, and gold-sputtered. Representative SEM images are shown in Figure 3. Frame (a) clearly supports our description of the aforementioned two-stage growth process. The left portion of the tube has a very smooth surface, while the curved right portion seems to consist of rings of bricklike units, which suggest the
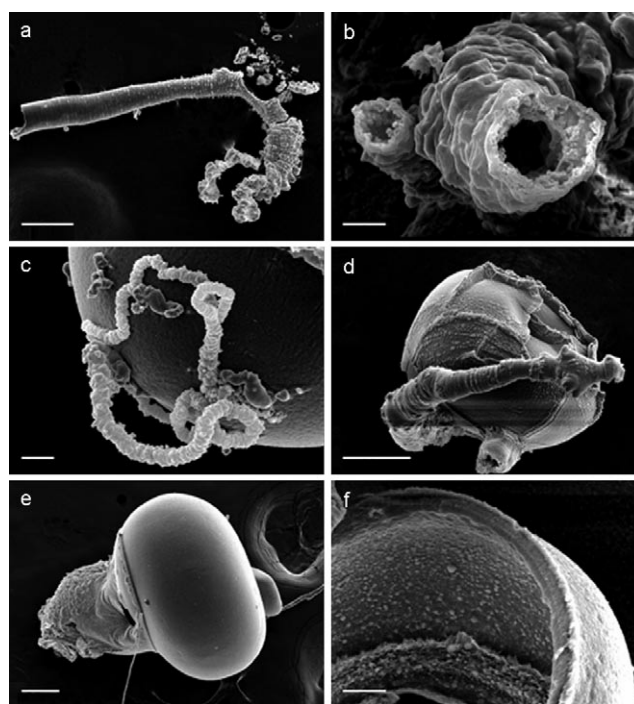
Figure 3. Scanning electron micrographs of microstructures. a) Tube fragment showing the transition from smooth to coarse morphology. b) View of the tubes' hollow cross-section. c) Small tube attached to spherical shell. d) Larger tube on shell with "self-healed" fractures. e) Shell with large nodular growth and a very thin tube. f) Cross-section of a typical shell wall. [CuSO$_4$] = 1.0 M. Scale bars: 100 μm (a, d, e), 10 μm (b, f), 20 μm (c).

presence of small crystallites. One can therefore speculate that the slower growth favors crystallization over amorphous precipitation. Frame (b) shows two microtubes from a viewpoint that reveals details of the tubes' cross-section, and establishes that the tubes are indeed hollow and remain hollow even after reaching their final length. The typical wall thickness is less than 2 μm and the inner surface appears to be more rugged than the outer one. The thinner tube in Figure 3b has an inner radius of approximately 3 μm.

Frames (c) and (d) in Figure 3 show tubes that remained attached to the shell of the microbeads. The tube in frame (c) is very long compared to its diameter and stayed close to its reagent-delivering microbead. We note that thin and slow-growing tubes often follow external surfaces, back-trace their own path, or grow short segments in a helical fashion. It is also noted that the surface of the spherical shell in Figure 1c is very smooth. In other cases, however, the shell surface has pronounced ridges. As can be seen by comparing Figures 1f and 3d, it is likely that these ridges are caused during the fracturing and reaction-induced "self-healing" of the forming shell. The tube in Figure 3d is also interesting as it features a slightly different surface morphology. Here the tube appears to be segmented into smooth ring-like segments and terminates in a remarkable structure that resembles a spikelike club or mace.

The SEM images in Figure 3e, f show additional details of the observed microstructures. Frame (e) shows one of the nodular structures that we described in the context of

Figures 1 a–d. The rugged surface of this nodular growth is in stark contrast to the smooth surface of the main shell. Furthermore, the base of these nodules is a near-perfect circle. The thin, straight tube in the lower half of the image became detached from the small hole in the middle of the frame during preparation. Figure 3 f shows a cross-section of a shell wall. The rim of the wall is a very clean, circular fracture that possibly arises from a detached nodular growth. The shell wall has a thickness of 6 μm and is therefore three times thicker than microtube walls. We note that earlier studies of macroscopic tubes revealed that the interior and exterior wall consists primarily of copper hydroxide and amorphous silica, respectively,[13] and expect our materials to have the same layered composition.

All experiments discussed up to this point involve situations in which the reagent-loaded microbead maintained a stationary position. However, we observed numerous times that it was not the bubble but the reagent-loaded microbead that moved in response to the forming tube. This scenario occurs if the tube is pinned to the air/silicate solution interface or to larger air bubbles that themselves are pinned to the surface of the reaction vessel. The four consecutive snapshots in Figure 4 illustrate these dynamics. In this example, the polymer bead moves 430 μm in 38 s to yield an average speed
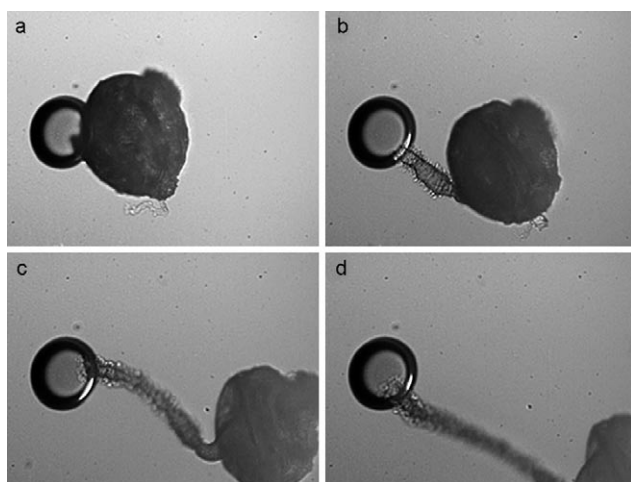
Figure 4. Sequence of optical micrographs showing a self-propelled microbead. The growing tube connects the bead to a stationary air bubble. Time elapsed between subsequent frames is 13 s. Images show an area of (0.62×0.47) mm². [CuSO₄]=1.0 м.

of 11 μm s⁻¹. This speed falls well within the range of the slow growth velocities shown in Figure 2 b. Also, the segmented tube morphology is indicative of the slow, erratic growth regime. In addition, movies of such experiments reveal that tube growth occurs directly at or close to the bubble surface. The actual point of contact between tube and bubble is not stationary but moves slightly and in an erratic fashion over the bubble surface. The tube–bead system can also rotate with respect to the bubble. We did not find obvious differences between microtubes formed from stationary and nonstationary beads. In addition, we did not observe buckling or any other unusual deformations of the bead-pushing tubes. The

latter observation, along with the similarities in speed between moving bubbles (Figure 2 b) and moving beads (Figure 4) indicate that the propulsion velocity of the bead is not affected by viscous forces. For the bead radii and solution viscosity (1.74 cP)[14] investigated, the tubular propulsion system does, therefore, not work at maximal load and the forming tube should be capable of moving larger objects.

The latter type of microbead motion associates our reaction with a larger group of nano- and micrometer-sized systems that utilize chemical reactions to perform directional motion. Such self-propelled chemical entities include biomotors, nanodimers, Au/Pt nanorods, and certain reacting polymers.[15] Our system, however, is unique in the sense that the actual "motor" of the translational motion remains near-stationary, while its fuel reservoir moves by extending a hollow conduit. The microbead velocities and radii are comparable to those of many living cells.[16]

In conclusion, we have developed a simple procedure for producing hollow silica/metal hydroxide microshells and microtubes, which can be fully controlled by the reactant's initial confinement and total dose. The spatial and temporal scales involved allow detailed studies of the growth process and underlying mechanisms. Preliminary results suggest that this technique can be generalized to a wide range of materials. Moreover, the high aspect ratio and small radii (only several micrometers) of the tubes should allow for interesting applications in microfluidics and other technologies, especially because the structures are sturdy enough to withstand alterations of their composition and surface structure. However, more work is needed to maintain microtube growth over longer distances. We believe that this problem could be solved by delivering salt solution diffusively through the polymer bead from a large reservoir into the silicate solution. Such a ballpoint-pen-like device would allow the production of very long and shape-specific microtubes in a three-dimensional writing process.

Experimental Section

All chemicals were of analytical grade and used without further purification. Agarose microbeads were prepared using a water-in-oil (W/O) emulsification technique.[7] A 4 wt% aqueous solution of agarose (containing 0.9 wt% sodium chloride) at around 75°C was dispersed in a hot oil phase (65°C). The oil phase consisted of a mixture of liquid paraffin and petroleum ether (7:5 v/v) and contained 4 wt% of the surfactant Span 80. The dispersed agarose droplets solidified as they were cooled to room temperature under continuous rapid stirring. The resulting hydrophilic microbeads partitioned into the aqueous phase and could be easily removed. The beads were polydisperse with radii in the range of 1.5 to 500 μm.

The as-formed agarose microbeads were soaked in copper sulfate solution of different concentrations for about 24 h. The range of concentrations employed was 0.070 to 1.15 mol L⁻¹. All aqueous solutions were prepared in nanopure water (18 MΩ cm; EASYpure UV, Barnstead). The loaded beads were extracted from the copper sulfate solution and spread in a Petri dish. After approximately 10 min of ambient air drying, a solution of sodium silicate (1.0 м) was added over the loaded beads, and shells and tubes started to form. In all experiments, the concentration of sodium silicate was kept constant at 1.0 м.

Communications

During and after the experiment, optical micrographs were acquired with a charge-coupled device camera (COHU 2122) connected to an inverted microscope (Leica, DM IRB). Image sequences were captured using HLImage + + 97 software at a typical rate of 3.3 frames per second. For further characterization, shells and tubes were removed from the sodium silicate solution, washed three to four times with water, and then air-dried at room temperature. The specimens were placed in a vacuum dessicator to remove the remaining moisture, and were gold sputtered to enhance the conductivity of the surface. SEM images were obtained on a JEOL JSM-5900 scanning electron microscope.

[1] See, for example:S. Mann *Biomineralization*, Oxford University Press, Oxford, **2001**.

[2] K. J. C. van Bommel, A. Friggeri, S. Shinkai, *Angew. Chem.* **2003**, *115*, 1010–1030; *Angew. Chem. Int. Ed. Engl.* **2003**, *42*, 980–999.

[3] a) J. H. E. Cartwright, J. M. García-Ruiz, M. L. Novella, F. Otálora, *J. Colloid Interface Sci.* **2002**, *256*, 351; b) J. Pantaleone, A. Toth, D. Horvath, J. R. McMahan, R. Smith, D. Butki, J. Braden, E. Mathews, H. Geri, J. Maselko, *Phys. Rev. E* **2008**, *77*, 046207.

[4] a) D. D. Double, A. Hellawell, S. J. Perry, *Proc. R. Soc. London Ser. A* **1978**, *359*, 435; b) D. A. Stone, R. E. Goldstein, *Proc. Natl. Acad. Sci. USA* **2004**, *101*, 11537.

[5] C. Ritchie, G. J. T. Cooper, Y.-F. Song, C. Streb, H. Yin, A. D. C. Parenty, D. A. MacLaren, L. Cronin, *Nat. Chem.* **2009**, *1*, 47–52.

[6] a) H. Nakamura, Y. Matsui, *J. Am. Chem. Soc.* **1995**, *117*, 2651–2652; b) F. Miyaji, S. A. Davis, J. P. H. Charmant, S. Mann, *Chem. Mater.* **1999**, *11*, 3021–3024; c) H.-P. Lin, S. Cheng, C.-Y. Mou, *Chem. Mater.* **1998**, *10*, 581–589.

[7] a) S. Hjerten, *Biochim. Biophys. Acta Spec. Sect. Biophys. Subj.* **1964**, *79*, 393–398; b) Q.-Z. Zhou, L.-Y. Wang, G.-H. Ma, Z.-G. Su, *J. Colloid Interface Sci.* **2007**, *311*, 118–127.

[8] a) S. Thouvenel-Romans, O. Steinbock, *J. Am. Chem. Soc.* **2003**, *125*, 4338; b) D. A. Stone, B. Lewellyn, J. C. Baygents, R. E. Goldstein, *Langmuir* **2005**, *21*, 10916–10919.

[9] a) S. Thouvenel-Romans, J. J. Pagano, O. Steinbock, *Phys. Chem. Chem. Phys.* **2005**, *7*, 2610; b) J. J. Pagano, T. Bánsági, Jr., O. Steinbock, *Angew. Chem.* **2008**, *120*, 10048–10051; *Angew. Chem. Int. Ed. Engl.* **2008**, *47*, 9900–9903.

[10] J. R. Gladden, A. Belmonte, *Phys. Rev. Lett.* **2007**, *98*, 224501.

[11] a) R. P. Wool, *Soft Matter* **2008**, *4*, 400–418; b) D. Y. Wu, S. Meure, D. Solomon, *Prog. Polym. Sci.* **2008**, *33*, 479–522.

[12] O. V. Yarovaya, K. I. Kienskaya, V. V. Nazarov, *Colloid J.* **2004**, *66*, 367–371.

[13] a) D. Balköse, F. Özkan, U. Köktürk, S. Ulutan, S. Ülkü, G. Nişli, *J. Sol-Gel Sci. Technol.* **2002**, *23*, 253; b) J. J. Pagano, S. Thouvenel-Romans, O. Steinbock, *Phys. Chem. Chem. Phys.* **2007**, *9*, 110–118.

[14] S. Thouvenel-Romans, W. van Saarloos, O. Steinbock, *Europhys. Lett.* **2004**, *67*, 42–48.

[15] a) J. Maselko, P. Borisova, M. Carnahan, E. Dreyer, R. Devon, M. Schmoll, D. W. Douthat, *J. Mater. Sci.* **2005**, *40*, 4671–4673; b) F. Paxton, S. Sundararajan, T. E. Mallouk, A. Sen, *Angew. Chem.* **2006**, *118*, 5546–5556; *Angew. Chem. Int. Ed. Engl.* **2006**, *45*, 5420–5429; c) J. R. Howse, R. A. L. Jones, A. J. Ryan, T. Gough, R. Vafabakhsh, R. Golestanian, *Phys. Rev. Lett.* **2007**, *99*, 048102; d) Y. G. Tao, R. Kapral, *J. Chem. Phys.* **2008**, *128*, 164518.

[16] a) H. C. Berg, *Phys. Today* **2000**, *53*, 24–29; b) B. Alberts, A. Johnson, J. Lewis, M. Raff, K. Roberts, P. Walter, *Molecular Biology of the Cell*, Garland Science, New York, **2002**.